Article Type: Full Length Article

Indium Phosphide Based Solar Cell Using Ultra-Thin ZnO as an Electron Selective Layer

Vidur Raj[1,], Tâmara Sibele dos Santos[1], Fiacre Rougieux[2], Kaushal Vora[3], Mykhaylo Lysevych[3], Lan Fu[1], Sudha Mokkapati[4], Hark Hoe Tan[1,*] and Chennupati Jagadish[1]*

E-mail: vidur.raj@anu.edu.au; hoe.tan@anu.edu.au

[1]Department of Electronic Materials Engineering, Research School of Physics and Engineering, The Australian National University, Canberra, ACT 2601, Australia
[2]Department of Engineering, College of Engineering and Computer Science, The Australian National University, Canberra ACT 2601, Australia
[3]Australian National Fabrication Facility, Research School of Physics and Engineering, The Australian National University, Canberra, ACT 2601, Australia
[4] School of Physics and Astronomy, Cardiff University, Queen's Buildings, The Parade, Cardiff, CF 24 3AA, Wales, UK

Keywords: ZnO/InP interface; III-V; Heterojunction; SCAPS-1D Simulation; Solar Cell; Electron Selective Layer

Abstract

According to Shockley–Queisser limit the maximum achievable efficiency for a single junction solar cell is ~ 33.2 % which corresponds to a bandgap (E_g) of 1.35 eV (InP). However, the maximum reported efficiency for InP solar cells remain at 24.2 ± 0.5 %, that is >25 % below standard Shockley–Queisser limit. Through a wide range of simulations, we propose a new device structure, ITO/ ZnO/i-InP/p^+ InP (p-i-ZnO-ITO) which might be able to fill this efficiency gap. Our simulation shows that the use of a thin ZnO layer improves passivation of the underlying i-InP layer and provides electron selectivity leading to significantly higher efficiency when compared to their n^+/i/p^+ homojunction counterpart. As a proof-of-concept, we fabricated ITO/ZnO/i-InP solar cell on a p^+ InP substrate and achieved an open-circuit voltage (V_{oc}) and efficiency as high as 819 mV and 18.12 %, respectively, along with ~90% internal quantum efficiency. The entire device fabrication process consists of four simple steps which are highly controllable and reproducible. This work lays the foundation for a new generation of thin film InP solar cells based solely on carrier selective heterojunctions without the

requirement of extrinsic doping and can be particularly useful when p- and n-doping are challenging as in the case of III-V nanostructures.

1. Introduction

III-V semiconductors are ideal candidates for high efficiency solar cells because of their tuneable and direct band gaps. However, the high cost of III-V semiconductors have restricted their reach to the commercial market. There has been a lot of effort to reduce the overall cost of III-V solar cells while maintaining their high efficiency such as reduction of material usage (i.e. reducing the thickness of active region), simplification of processing steps, photon recycling, etc. [1-4] Amongst single junction solar cells, maximum efficiency of 28.8 ± 0.9 % has been reported for thin film GaAs solar cells.[5] However, despite InP being theoretically the most suitable candidate for single junction solar cells, its reported maximum efficiency remains at 24.2 ± 0.5% which is way below the Shockley-Queisser limit of InP and thus has a lot of room for improvement.[5, 6]

In a conventional p-n homojunction solar cells, doping is required to create a built-in electric field that facilitates the charge carrier separation and collection. However, these conventional doped devices are hindered by several optoelectronic losses such as parasitic absorption and Auger recombination together with technological limitations specific to doped semiconductors and fabrication complexities.[13] Some of these limitations can be overcome by using an intrinsic layer based heterojunction solar cell where heavily doped homojunctions are replaced by a wide band gap electron and/or hole selective contact layers. In these wide band gap carrier selective layers, such as TiO_2, ZnO, MoO_x, etc. [7-10], large conduction or valence band offset along with low intrinsic carrier concentration ensures a very small minority carrier conductivity under illumination.[11,13] Consequently, the surface recombination in the charge carrier selective layer and recombination at the oxide/metal interface is significantly reduced which in turn leads to efficient solar cell operation.[11] However, for efficient working of heterojunction solar cells the Oxide/absorber interface should be well passivated and free of any defects states in the forbidden gap of absorber layer.

There have been numerous studies on metal oxide based electron selective contacts for c-Si solar cells, [13, 14] however; there are very limited studies on III-V heterojunction solar cells. [8,10] Most recently, Yin et al. demonstrated TiO_2 as an efficient electron selective contact for p-type InP. [10] In this work, we use simulation and experiments to show ZnO as another potential candidate as an electron selective contact for InP solar cell. Firstly, we employ simulations to show potential advantages of ITO/ZnO/i-InP/p^+ InP (p-i-ZnO-ITO) heterostructure as compared to their $n^+/i/p^+$ (p-i-n) homojunction counterpart. Later, based on simulations, we fabricate p-i-ZnO-ITO heterojunction solar cells and demonstrate experimentally that this solar cell architecture allows for high near band edge quantum efficiency, with an overall efficiency of 18.12 % and a high V_{oc} of 819 mV. Our solar cells are mainly limited by optical, series and shunt losses which can be minimized with further optimization. The entire device fabrication process consists of four simple steps which are highly controllable and reproducible. Consistent with simulation results, our experimental data indicate that the high performance of such solar cells stem from high carrier selectivity of metal oxides and the passivation of i-InP by ZnO.

2. Simulation Methods and Experimental Details

Simulation: We used SCAPS-1D [15, 16] to perform the simulation of the p-i-n and p-i-ZnO-ITO solar cell structures that are shown schematically in Figure 1. In Figure 1, the interfaces between two subsequent layers is shown using a thin black line. Using this program, we calculate the energy bands, carrier concentrations and currents at a given voltage and a corresponding J-V (current density vs voltage) plot is obtained. Based on material parameters and defect concentration inputs, different recombination currents such as band-to-band (direct), Auger, Shockley-Read-Hall (SRH)-type, bulk and interface recombination currents are evaluated. Semiconductor parameters (such as electron affinity, doping, band gap, electron and hole mobility etc.) and defect levels were obtained from either published experimental results or from an online database. Details regarding the parameters and

references used during simulation are given in Tables S1 and S2 of the supplementary section. Simulations are performed both under ideal condition (no interface defects) and in presence of interface defects.

Fabrication: The procedure for the fabrication of p-i-ZnO-ITO solar cells started with the growth of a 2 µm i-InP layer on a 350 micron p^+-type (100) InP substrate using Metal-Organic Chemical Vapour Deposition (MOCVD). Next, an Ohmic contact was made on the back of p^+ InP wafer by alloying Zn:Au (10 nm:100 nm) at 400 °C in the presence of forming gas (5% H_2 and 95% N_2). Subsequently, to obtain high quality ZnO, different sputter parameters such as thickness, temperature and power, were varied. All sputter depositions were performed in an argon atmosphere at a pressure of 1.5 mTorr using a ZnO target. High temperature and low RF power were found to be important to achieve high quality devices. Based on initial optimization, temperature and power were fixed at 350 ^oC and 60 W respectively, and the thickness of ZnO was varied further to optimize the performance of these solar cells. The maximum temperature during ZnO deposition was limited to 350 °C to avoid phosphorus desorption from the InP wafer at temperatures higher than 380 °C. After each ZnO deposition, ITO was deposited at room temperature using an ITO target with an RF power of 100 W and a pressure of 1.5 mTorr with argon flow of 20 sccm. ITO was sputtered in the same sputter system such that the overall thickness of oxide layers (combined thickness of ZnO and ITO) remained at 70 nm. At around 70 nm of oxide thickness, the reflectance minimum falls in the spectral range where the solar spectrum is strongest (around a wavelength of 600 nm) in order to maximize light in-coupling into the InP absorber. [10] Also, ITO was required to make an Ohmic contact and to facilitate lateral current flow across the metal contact. Finally, Ti/Au (100 nm) top finger-contact was fabricated by photolithography and electron beam evaporation. After fabrication, a cell size of 0.9 x 0.9 cm^2 was cleaved manually using a precision diamond scriber for device measurements.

Characterization: To evaluate the device performance, current-voltage (I-V) measurement was performed using an Oriel Solar Simulator I-V test station. For each measurement, the solar simulator

was calibrated to 1 sun (100 mW/cm^2) at 25 ^{o}C using a silicon reference cell. External quantum efficiency (EQE) measurement was performed using a NewSpec IQE-200 AC system. To calculate internal quantum efficiency (IQE) of the solar cell, the reflectance was measured separately using a Shimadzu UV-3101PC UV-Vis-IR spectrophotometer. For surface characterization, X-ray photoelectron spectroscopy (XPS) and ultra-violet photoelectron spectroscopy (UPS) were performed in a Thermo ESCALAB250Xi X-ray photoelectron spectrometer. TRPL (time-resolved photoluminescence) measurement was performed using a Yb:YAG laser with a pulse duration of 300 fs, repetition rate of 20.8 MHz, frequency-doubled to a wavelength of 532 nm using a LBO crystal. A charge-coupled device array was used to record the photoluminescence (PL) spectrum with a spectrometer and a Picoharp 300 time-correlated single photon counting system used to detect the PL decay. TRPL intensity decay at peak wavelength was fitted by a single-exponential decay to extract the minority carrier lifetime. [17, 18]

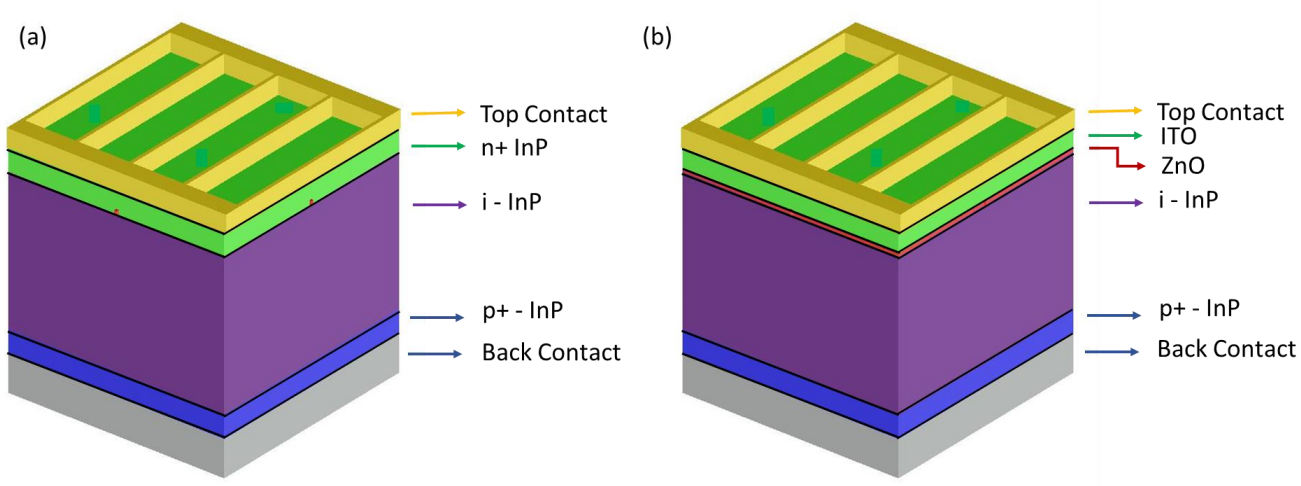

Figure 1. Schematic representation (not to scale) of the InP solar cell structures used for simulation (a) p-i-n and (b) p-i-ZnO-ITO. In both the figures, interface between two subsequent layers has been marked using a thin black line.

3. Results and Discussion

3.1. Simulation Results

To show the potential of ZnO as an electron selective contact for InP solar cells, in this section we present the simulation results for p-i-ZnO-ITO solar cell architecture and compare it to p-i-n InP homojunction solar cell architecture. The schematic representation of the two types of solar cell structures used for device simulation is shown in Figure 1. Figure 1(a) shows a p-i-n solar cell with 2 µm i-InP stacked between heavily doped 100 nm p^+ and n^+ InP layers while a p-i-ZnO-ITO solar cell structure is represented in Figure 1(b). In p-i-ZnO-ITO cell, 2 µm i-InP layer is stacked between a 100-nm p+ InP layer and a thin ZnO/ITO (70 nm) layer. During all the simulations, the total thickness of ZnO and ITO is maintained at 70 nm. For all the simulation results shown below, we maintain the ZnO thickness at 10 nm and ITO thickness at 60 nm, respectively.

The device characteristics along with the band diagrams of p-i-n and p-i-ZnO-ITO solar cells are shown in Figure 2. Figure 2(a) shows the simulated J-V characteristic of p-i-n and p-i-ZnO-ITO solar cells while the plots in Figure 2(b) show the corresponding band diagram of these devices under illumination at V_{oc}. As shown in Figure 2(a) and Table 1, the p-i-ZnO-ITO device outperforms p-i-n device both in terms of V_{oc} and J_{sc} and has a higher FF and efficiency. For p-i-n device a V_{oc} and J_{sc} of 960 mV and 30.4 mA/cm^2 was obtained in comparison to a V_{oc} and J_{sc} of 1030 mV and 33.6 mA/cm^2 obtained respectively for the p-i-ZnO-ITO solar cell.

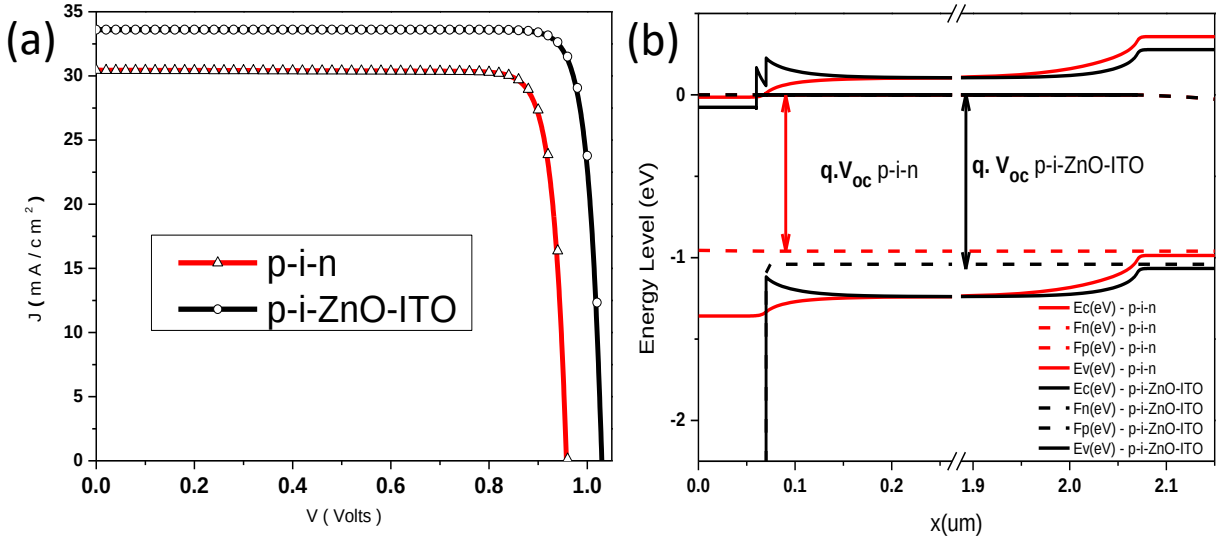

Figure 2. (a) Simulated J-V curve for p-i-n and p-i-ZnO-ITO solar cells in the absence of interface defects (b) Band diagram of p-i-n and p-i-ZnO-ITO solar cells under illumination at V_{oc}.

Samples	V_{oc} (m V)	J_{sc} (m A / c m ^{2})	FF (%)	Efficiency (%)
p-i-n	960	30.4	87.4	25.5
p-i-ZnO	1030	33.6	88.5	30.6

Table 1. Simulated solar cell performance parameters of p-i-n and p-i-ZnO-ITO solar cells obtained using SCAPS-1D in the absence of interface defects.

In steady state illumination condition, at V_{oc} (open-circuit voltage) the photogenerated free carriers accumulate at the respective contacts to constitute a potential difference that is equal to the V_{oc}. In general, V_{oc} can be written in terms of the splitting of electron and hole quasi-Fermi energy levels as:

$$V_{oc} = \frac{1}{q}\,(f_n - f_p)$$

Where, f_n and f_p are electron and hole quasi-Fermi levels. It is quite apparent from Figure 2(b) that a difference in the V_{oc} of p-i-ZnO-ITO and p-i-n solar cells is a direct consequence of large Fermi level splitting in p-i-ZnO-ITO as compared to p-i-n structures. An increase in V_{oc} of p-i-ZnO-ITO solar cells as compared to p-i-n solar cells is because of reduced recombination at the front contact as confirmed by the simulated recombination currents shown in Figure S1 of the supplementary section. This observation is in agreement to the previously reported results from Würfel et. al. [11] where a similar structure has been simulated and compared with p-i-n homojunction.

The curves in Figure 2 and performance parameters shown in table 1 are calculated for ideal conditions in the absence of interface defects. However, in real devices, interface defects may be higher for oxide/InP interface as compared to epitaxially-grown p-i-n solar cells. Hence, we

performed a comparative simulation between p-i-n and p-i-ZnO-ITO structures in the presence of interface defects. For p-i-n solar cells, the density of interface defects was set to zero as we expect very low interface defect density considering that these structures are usually grown using mature epitaxial techniques. Furthermore, according to previous reports, [22, 23] for oxide/InP interface two defect levels have been reported at 0.39 and 0.51 eV below the conduction band minima (CBM), respectively with a capture cross section of 1×10^{-17} and 1×10^{-12} cm^2.[23]

During simulation, peak Gaussian interface defect density for each of these defect states were varied from 1 x 10^{10} cm^{-2} eV^{-1} to 1 x 10^{15} cm^{-2} eV^{-1}. Table S3 in the supplementary section shows the change in solar cells performance parameter of p-i-ZnO-ITO solar cells with a change in interface defect density. As expected, we find that ultimate efficiency of p-i-ZnO-ITO solar cells depends critically on the defect density at the ZnO/InP interface. Significant degradation in efficiency can be seen when any one of these interface defect states has a density of more than 10^{14} cm^{-2} eV^{-1}. This decrease in efficiency is a combined effect of loss of carriers through interface recombination that leads to a decreased J_{sc} and an increased total recombination current which reduces V_{oc}. However, even in presence of a peak Gaussian defect density of up to 10^{13} cm^{-2} eV^{-1} for both the aforementioned defects, p-i-ZnO-ITO solar cells perform better than an ideal p-i-n solar cell.

Through a wide range of simulations, we conclude that the p-i-ZnO-ITO cell is more advantageous than the p-i-n cell in three main aspects: 1) Higher current due to very low absorption loss in the ZnO-ITO top layer, while light absorption in the (100 nm) n^+-InP layer leads to a loss of current of ~3 mA/cm^2; 2) Higher voltage because of reduced recombination at the front contact; and 3) p-i-ZnO-ITO solar cells can outperform their p-i-n counterparts even in the presence of moderate density of defects at the ZnO/i-InP interface.

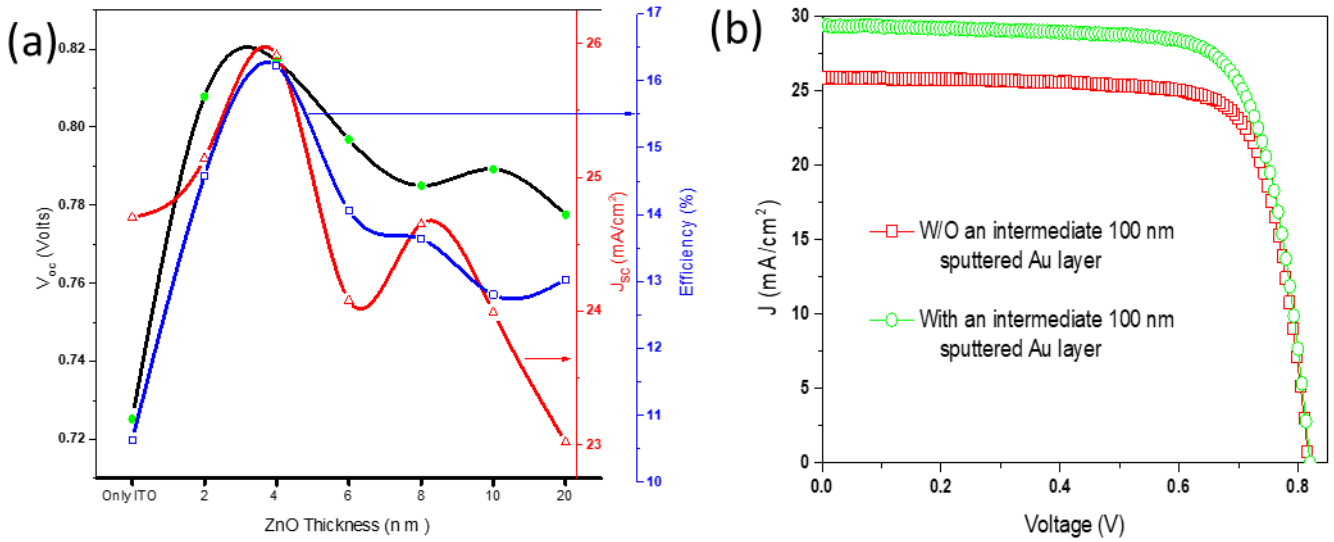

Figure 3. (a) Optimization of ZnO thickness for the p-i-ZnO-ITO solar cells without a 100 nm sputtered Au between ITO and Ag. Voc, Jsc and FF are shown using arrows directed to different y-axes. (b) J-V curve for the p-i-ZnO-ITO (with 4nm ZnO thickness) solar cell fabricated with and without a 100 nm sputtered Au between ITO and Ag.

3.2. Optimization of ZnO

In this section we show the effect of thickness of ZnO on the performance of p-i-ZnO-ITO solar cells. Figure 3 (a) shows J_{sc}, V_{oc} and efficiency plotted against the variation in ZnO thickness. A ZnO layer of 4 nm thickness shows maximum efficiency with V_{oc} and J_{sc} values of 817 eV and 25.91 mA/cm^2, respectively. However, decreasing the thickness further to 2 nm reduces V_{oc} and J_{sc} and beyond 10 nm of ZnO thickness V_{oc} and J_{sc} are below 789 mV and 23.99 mA/cm^2, respectively. A decrease in V_{oc} and J_{sc} with increased thickness is probably because of an increased fixed charge density at the ZnO/InP interface. [21] An increase in fixed charge density with increased thickness, increases the ZnO work function [19, 21] and changes the ITO/InP barrier height which adversely affects the V_{oc}, and J_{sc} of solar cells. [19-21] Moreover, below a certain thickness, the coverage of ZnO is likely to be non-uniform, hence leading to an optimum thickness of 4 nm.

Furthermore, during fabrication, we found that a layer of sputtered gold (Au) between ITO and e-beam evaporated silver (Ag) contact significantly improves J_{sc}. This improvement is mainly because of improved charge collection at the front contact due to increased adhesion (confirmed by "scotch tape" test) of the top metal contact with ITO. Keeping that in mind, our best device was fabricated with 4 nm ZnO and the top contact was made using 100 nm sputtered Au followed by 100 nm of e-beam evaporated Ag over ITO. The use of a 100 nm sputtered Au layer between ITO and Ag improves J_{sc} significantly from 25.91 mA/cm^2 to 29.40 mA/cm^2, while maintaining the V_{oc}. A J-V characteristic corresponding to solar cells with and without a 100 nm sputtered Au between ITO and Ag is shown Figure 3(b). For our best solar cell, we obtain 18.12 (± 0.5) % efficiency with a V_{oc}, J_{sc} and FF of 819 mV, 29. 40 mA/cm^2, and 75.23 %, respectively. To test the reproducibility of the process, five different samples were fabricated and tested. Results along with mean and standard deviation in the solar cell characteristic parameters are given in Table S4 of the supplementary section. It is evident that the efficiency of these solar cells are quite reproducible within a range of 17.66 ±0.5 %. The efficiency of these cells can be further improved by increasing the fill factor which is ~ 75% for our best solar cell. This low fill factor is mainly because of high series resistance (~ 3.2 Ω cm^2) and low shunt resistance (~1500 Ω cm^2). The high series resistance is mainly due to relatively thin metal contacts over ITO whereas shunt resistance is mainly related to cleaving and processing of samples. Significant improvement can be expected in a cell fabricated with thick metal contacts, cleaved using lasers or mesa etched.

3.3. Characterization of p-i-ZnO-ITO solar cells

3.3.1 External Quantum Efficiency

The external quantum efficiency (EQE) along with reflectance and internal quantum efficiency (IQE) of our best performing solar cell is plotted in Figure 4. Internal quantum efficiency was calculated using the following equation: [27]

$$IQE = EQE/A = EQE/(1-T-R) \approx EQE/(1-R)$$

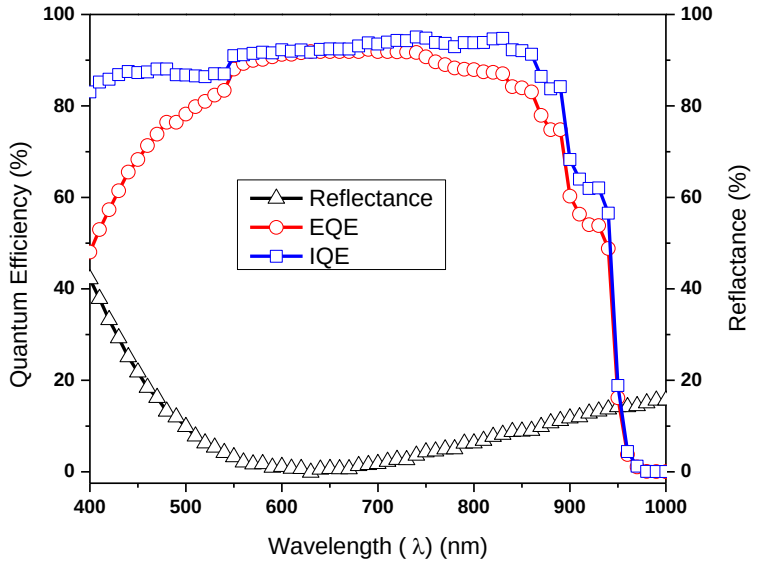

Figure 4. Quantum efficiencies and reflectance measured from p-i-ZnO-ITO solar cells.

In the above equation, A, T and R, are absorption, transmission and reflectance, respectively. EQE of the p-i-ZnO-ITO solar cell is between 85-90 % in most of the wavelength region of the spectrum and stays at 80% in the near band edge region. The relatively low external quantum efficiency in shorter wavelength region stems from surface related losses such as surface/interface defect mediated recombination and lateral charge carrier transport losses along with absorptive and reflective losses from ITO/ZnO layer. The high quantum efficiency in the longer wavelength region (> ~600 nm) is due to the use of a high quality i-InP absorber layer which ensures minimum bulk carrier recombination. The internal quantum efficiency, plotted in red in Figure 4, is at ~ 90% throughout the measured wavelength region and exceeds 90% in near band edge region which is mainly due to reduced rear interface recombination that is a combined effect of high absorption coefficient of InP and homoepitaxy which ensures minimal carrier recombination near the i-InP/substrate interface. Based on our calculations, just by reducing optical losses (for example, by using a ZnS/MgF_2 double anti-reflective layer) J_{sc} values may exceed 32 mA/cm^2 and significant improvement in efficiency can be realized.

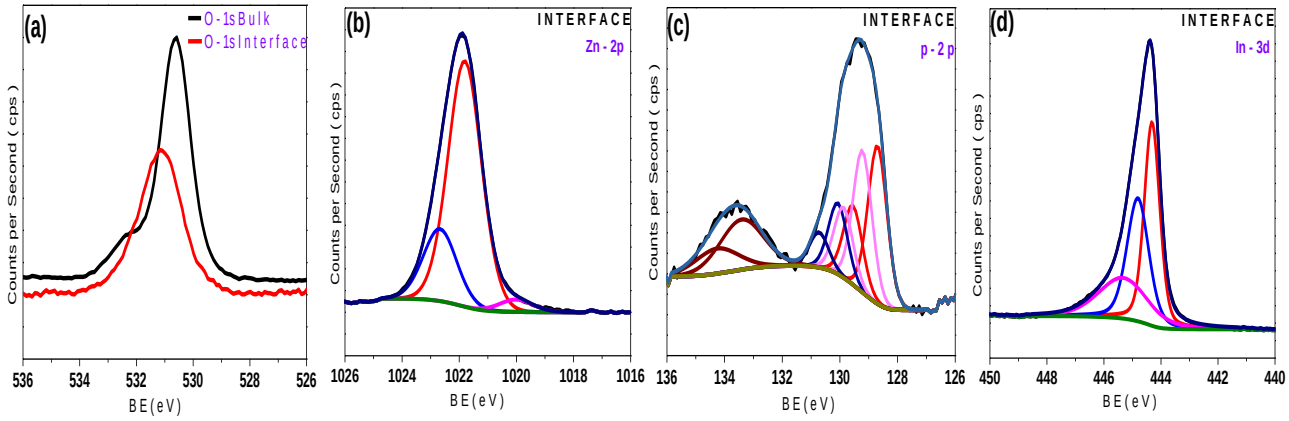

Figure 5. XPS spectra of (a) O-1s in bulk ZnO and at the ZnO/InP interface (b) Zn-2p at the ZnO/InP interface, (c) P-2p spectra at the ZnO/InP interface, and (d) In- $3d^{5/2}$ spectra at the ZnO/InP interface

3.3.2 Chemical properties of the interface with X-ray photoelectron spectroscopy (XPS) & TRPL

To determine the chemical properties of the ZnO/InP interface and thus further understand the passivation properties of ZnO we performed XPS, UPS and TRPL measurements.

ZnO/InP Interface

Figure 5(a) shows a comparative O-1s spectra for the bulk ZnO and ZnO/InP interface. A broadening in the O-1s XPS spectrum of ZnO/InP interface as compared to ZnO bulk and a shift towards higher binding energy side suggest the formation of new bonds and presence of more than one kind of oxygen species. It is quite evident that the overall peak has shifted towards high energy levels centred at ~ 531.2 eV. This shift suggests the presence of In-O type bonding (centred at ~531 eV) and an increase in non-stoichiometric composition of ZnO (centred at ~ 532 eV). The shift towards higher energy side in O-1s spectra agrees with a previously reported signal for $(P_2O_5)_x(ZnO)_{1-x}$[28]. Deconvoluted Zn-2p, P-2p and In-3d spectra for ZnO/InP interface are shown in Figure 5(b)-5(d), respectively. As can be seen in Figure 5(b) non-stoichiometric ZnO composition at ~ 1023.1 eV has increased significantly compared with bulk spectra (see supplementary section Figure S3). This suggests the breaking of stoichiometric Zn-O bonds to form new bonds. For the deconvoluted spectra

of bulk InP and ZnO please refer to figure S3 of the supplementary section. As also can be seen from deconvolution of P-2p spectrum at ZnO/InP interface shows three doublets in the range of 128 to 131.5 eV, and a satellite peak between 132 to 136 eV. The doublet at 128.3 eV is due to Zn-P type of bonding that is also seen in Zn_3P_2 materials whereas the doublet at 129.0 eV corresponds to In-P bonds. [30, 31] A small peak at 130.0 eV corresponds to elemental phosphorus. Formation of a new broad peak at ~133.2 eV is characteristic peak for oxidised InP that corresponds to phosphorus oxides such as $In(PO)_x$ and P_2O_5. [29,32] Oxidation of InP is further confirmed by deconvolution of In-$3d_{5/2}$ shown in figure 5(d). Deconvoluted In-$3d_{5/2}$ XPS spectra for ZnO/InP interface shows peaks centred at 443.7 eV, 444.2 and 444.73 eV corresponding to In-P, In-O and $In(PO)_x$, respectively. [28,29] A similar kind of shift and broadening at higher energy (compared to the bulk InP as shown in Figure S3(d)) were reported for InP in oxidation condition**.** [28, 29] These XPS results confirm the oxidation of InP and formation of $In(PO)_X$ bonds at ZnO/InP interface. Similar kind of XPS spectral changes in core levels of In-3d, and P-2p have been reported for high performance ITO/InP devices. [33]

3.3.3. Electronic property of the interface with ultraviolet photoelectron spectroscopy (UPS) analysis

To better understand the electrical properties and in particular the band diagram of the ZnO/i-InP interface we performed UPS and the corresponding plot is shown in Figure 6. The Fermi levels for all the samples were calibrated using a silver sample as the reference and the valence band maxima (VBM) was estimated by extrapolating the valence band contribution. For bulk i-InP, VBM was found at 0.9 eV below the Fermi edge which is very close to previously estimated values for InP(100) substrates.[34] In a similar fashion VBM for ZnO/i-InP cell was estimated to be 3.2 eV below the Fermi level as shown in Figure 6(a). The work function for a given interface can be calculated using the secondary electron onset energy ($E_{cut\text{-}off}$) on the binding energy scale using the equation

$$\Phi = h\nu - (E_{Cutoff} - E_{Fermi})$$

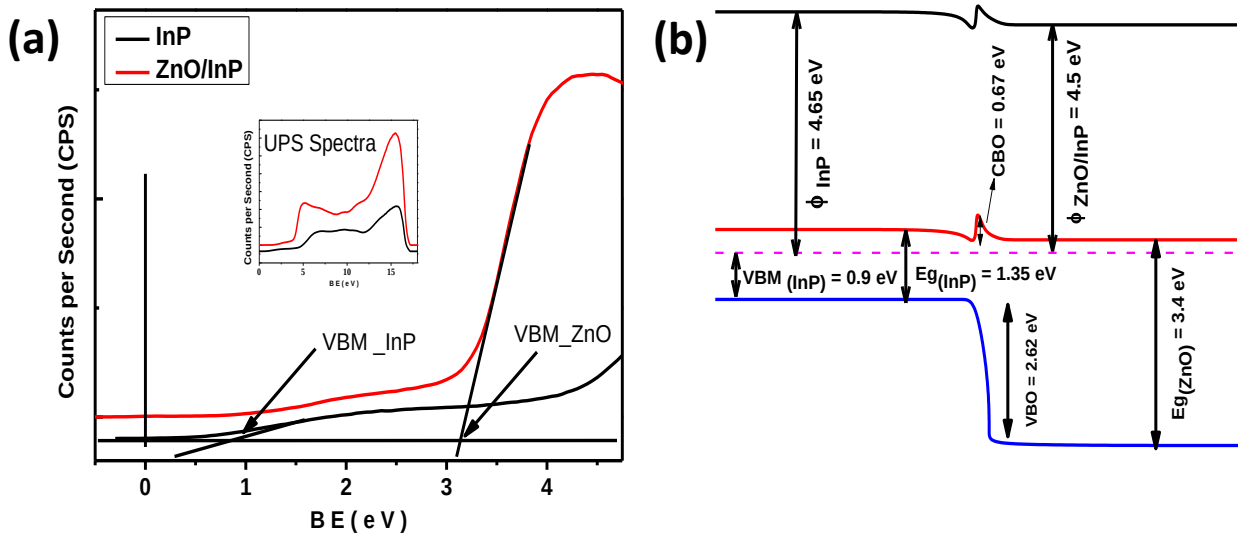

Figure 6. Comparative UPS spectra of (a) valence band maxima of bulk i-InP and ZnO/i-InP. Inset shows the UPS spectra for bulk i-InP (black) and ZnO/i-InP (red). (b) Band diagram at the ZnO/i-InP interface.

In above equation $h\nu$ denotes the energy of He-I line (21.22 eV) used in UPS. The Fermi energy, E_{Fermi} has been corrected for the interface and the bulk sample using a standard silver sample to 0 eV. We obtained a work function of 4.65 eV for bulk i-InP and a corresponding work function value for ZnO/i-InP was found to be 4.5 eV. This value of work function is similar to the one previously reported for bulk ZnO. [37] A band diagram constructed based on UPS spectra taken for i-InP and ZnO/i-InP sample is shown in Figure 6(b). The difference between the vacuum level ΔE_{vac} was obtained by subtracting the work function of i-InP and ZnO/i-InP, respectively. The valence band offset (VBO) was then calculated using:

$$\Delta E_v = \Delta e_v^{bulk} - (\Delta E_{InP} + \Delta E_{ZnO})$$

where, ΔE_{InP} is the difference in core level of In $3d_{5/2}$ for bulk i-InP and ZnO/i-InP , ΔE_{ZnO} is the difference in core level of Zn $2p_{3/2}$ for bulk ZnO and ZnO/i-InP and Δe_v^{bulk} is the difference between VBM of bulk ZnO and i-InP, respectively. ΔE_{InP} and ΔE_{ZnO} were calculated to be 0.5 and 0.02 eV, respectively, based

on XPS results shown earlier and using the above equation VBO is calculated to be 2.62 eV. The corresponding conduction band offset (CBO) was then calculated using the formula:

$$\Delta \text{ Ec} = \Delta E_{\text{vac}} + [\text{ Eg (ZnO)} - \text{Eg (InP)} - \text{VBO}]$$

Where, ΔE_{vac} is the difference in the work function of bulk i-InP and ZnO/i-InP. The bandgaps of ZnO and InP were assumed as 3.4 and 1.35 eV, respectively, leading to a conduction band offset of 0.67 eV. The calculated CBO introduces a spike at the ZnO/i-InP interface. A small spike of ~0.17 eV may be surmounted by photogenerated carriers but can still reduce the interface recombination significantly.

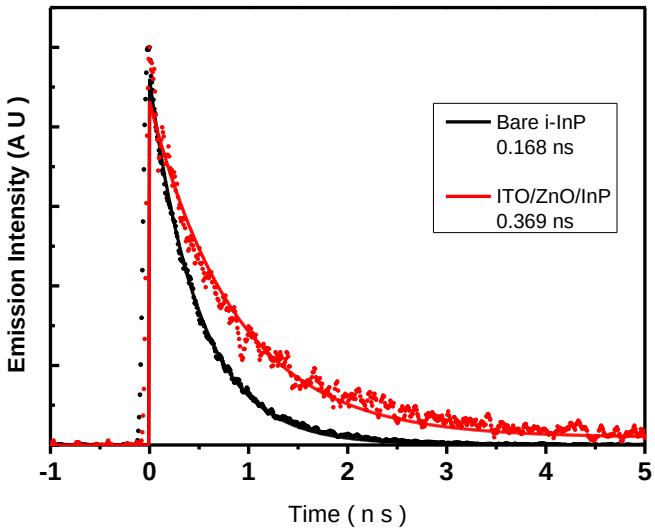

Figure 7. Comparison of carrier lifetime between bare i-InP and Oxide/i-InP sample. The lifetime values in the legend were obtained by a single exponential fit to the data.

Figure 7 shows the comparative fitted TRPL measurement data for both samples. It is quite evident that the carrier lifetime of oxide/i-InP is significantly higher than that of bare i-InP and confirms an improvement at the interface. Lifetimes calculated for bare i-InP and ZnO/i-InP are 0.168 and 0.3699 ns, respectively. Based on XPS results which show the formation of new bonds at the ZnO/InP interface and UPS results which show the band alignment of InP/ZnO, we can conclude that a combination of both

surface passivation for the InP surface as well as a large valence band offset at ZnO/i-InP interface result in the increased carrier lifetime, which agrees with previously reported results. [33-35]

4. Conclusions

In conclusion, we demonstrate the potential of p-i-ZnO-ITO InP solar cells in comparison to their p-i-n homojunction counterpart. Through device simulations it is found that the introduction of a large band gap n-type metal oxide (ZnO) over i-InP significantly improves solar cell performance parameters as compared to p-i-n homojunction solar cells because of increased carrier selectivity and improved passivation. It is also revealed that the presence of high density of interface defects may significantly degrade device performance but nevertheless, with a defect density of up to 10^{13} cm^{-2} eV^{-1} the p-i-ZnO-ITO InP solar cells may still outperform the p-i-n counterpart. As a proof-of-concept device, we fabricated ITO/n-ZnO/i-InP/p^+ InP solar cells and through initial optimization of oxide layer we obtain a V_{oc} of 819 mV and an efficiency of 18.1%. Quantum efficiency measurement shows internal quantum efficiency >90% which suggests good electronic behaviour of these solar cells. Furthermore, a carrier lifetime measurement shows improved minority carrier lifetime which supports the passivation of i-InP surface with ZnO layer. A combined XPS and UPS study suggests that passivation at ZnO/InP interface is mainly due to oxidation of InP surface as well as a large valence band offset at ZnO/i-InP interface. Although our results are still below that of the highest reported homojunction InP solar cell (efficiency = 22.1 %, V_{oc} = 0.878 V, J_{sc} = 29.3 mA/cm^2, and fill factor = 82 % [5]), it paves the way for using metal oxide as a selective contact to improve the performance of III-V solar cells, particularly when p- and n-doping are challenging as in the case of III-V nanostructures.

ASSOCIATED CONTENT

Supporting Information: Material parameters used during simulation; defect states at the ZnO/InP interface and its effects on the solar cell performance parameters; other simulation results such as recombination currents in ideal p-i-n and p-i-ZnO-ITO solar cell; generation plot; XPS of bulk ZnO; table showing reproducibility of our solar cells.

AUTHOR INFORMATION

Corresponding Author

*vidur.raj@anu.edu.au; hoe.tan@anu.edu.au

Author Contributions

The manuscript was written through contributions of all authors. All authors have given approval to the final version of the manuscript.

ACKNOWLEDGEMENTS

This research is supported by the Australian Research Council. The Australian National Fabrication Facility established under the Australian Government National Collaborative Research Infrastructure Strategy, is gratefully acknowledged for providing access to the epitaxial and fabrication facilities used in this work. We would like to acknowledge Prof. Andres Cuevas for a fruitful discussion that helped improve the paper. Tamara S Santos would like to acknowledge financial support from the "Programa Ciencias Sem Fronteiras and Capes".

REFERENCES

(1) Savage, N. Photon Recycling Breaks Solar Power Record. *IEEE Spectr.* **2011**, *48* (8), 16–16.

(2) Bauhuis, G. J.; Mulder, P.; Haverkamp, E. J.; Schermer, J. J.; Bongers, E.; Oomen, G.; Köstler, W.; Strobl, G. Wafer Reuse for Repeated Growth of III-V Solar Cells. *Prog. Photovoltaics Res. Appl.* **2010**, *18* (3), 155–159.

(3) Kosten, E. D.; Atwater, J. H.; Parsons, J.; Polman, A.; Atwater, H. A. Highly Efficient GaAs Solar Cells by Limiting Light Emission Angle. *Light Sci. Appl.* **2013**, *2* (1), e45.

(4) Eyderman, S.; John, S.; Smith, A.; Warta, W.; Dunlop, E. D. Light-Trapping and Recycling for Extraordinary Power Conversion in Ultra-Thin Gallium-Arsenide Solar Cells. *Sci. Rep.* **2016**, *6* (1), 28303.

(5) Green, M. A.; Hishikawa, Y.; Dunlop, E. D.; Levi, D. H.; Hohl-Ebinger, J.; Ho-Baillie, A. W. Y. Solar Cell Efficiency Tables (Version 51). *Prog. Photovoltaics Res. Appl.* **2018**, *26* (1), 3–12.

(6) Rühle, S. Tabulated Values of the Shockley-Queisser Limit for Single Junction Solar Cells. *Sol. Energy* **2016**, *130*, 139–147.

(7) Montgomery, K. H.; Nian, Q.; Zhao, X.; Li, H. U.; Cheng, G. J.; Jackson, T. N.; Woodall, J. M. Development of ZnO-InP Heterojunction Solar Cells for Thin Film Photovoltaics. In *2014 IEEE 40th Photovoltaic Specialist Conference (PVSC)*; IEEE, **2014**; pp 0524–0527.

(8) Pande, K. P.; Manikopoulos, C. N. ZnO□p-InP Heterojunction Solar Cells. *Sol. Cells* **1981**, *4* (2), 147–152.

(9) Battaglia, C.; Yin, X.; Zheng, M.; Sharp, I. D.; Chen, T.; McDonnell, S.; Azcatl, A.; Carraro, C.; Ma, B.; Maboudian, R.; et al. Hole Selective MoO_x Contact for Silicon Solar Cells. *Nano Lett.* **2014**, *14* (2), 967–971.

(10) Yin, X.; Battaglia, C.; Lin, Y.; Chen, K.; Hettick, M.; Zheng, M.; Chen, C.-Y.; Kiriya, D.; Javey, A. 19.2% Efficient InP Heterojunction Solar Cell with Electron-Selective TiO_2 Contact. *ACS Photonics* **2014**, *1* (12), 1245–1250.

(11) Wurfel, U.; Cuevas, A.; Wurfel, P. Charge Carrier Separation in Solar Cells. *IEEE J. Photovoltaics* **2015**, *5* (1), 461–469.

(12) Streetman B., Banerjee S., Chapter 4 & 5, *Solid State Electronic Devices (7th ed.),* **2015,** Pearson Education

(13) Bullock, J.; Hettick, M.; Geissbühler, J.; Ong, A. J.; Allen, T.; Sutter-Fella, C. M.; Chen, T.; Ota, H.; Schaler, E. W.; De Wolf, S.; et al. Efficient Silicon Solar Cells with Dopant-Free Asymmetric Heterocontacts. *Nat. Energy* **2016**, *1* (3), 15031.

(14) Bullock, J.; Kiriya, D.; Grant, N.; Azcatl, A.; Hettick, M.; Kho, T.; Phang, P.; Sio, H. C.; Yan, D.; Macdonald, D.; et al. Superacid Passivation of Crystalline Silicon Surfaces. *ACS Appl. Mater. Interfaces* **2016**, *8* (36), 24205–24211.

(15) M. Burgelman,, K. Decock, A. Niemegeers, J. Verschraegen, & S. Degrave, SCAPS Manual, (December), **2017**, 1–111.

(16) Burgelman, M.; Decock, K.; Khelifi, S.; Abass, A. Advanced Electrical Simulation of Thin Film Solar Cells. *Thin Solid Films* **2013**, *535*, 296–301.

(17) Gao, Q.; Saxena, D.; Wang, F.; Fu, L.; Mokkapati, S.; Guo, Y.; Li, L.; Wong-Leung, J.; Caroff, P.; Tan, H. H.; et al. Selective-Area Epitaxy of Pure Wurtzite InP Nanowires: High Quantum Efficiency and Room-Temperature Lasing. *Nano Lett.* **2014**, *14* (9), 5206–5211.

(18) Zhong, Z.; Li, Z.; Gao, Q.; Li, Z.; Peng, K.; Li, L.; Mokkapati, S.; Vora, K.; Wu, J.; Zhang, G.; et al. Efficiency Enhancement of Axial Junction InP Single Nanowire Solar Cells by Dielectric Coating. *Nano Energy* **2016**, *28*, 106–114.

(19) D. Moerman, H. Kim, A. E. Colbert, S. Graham, D. S. Ginger, The impact of ultra-thin titania interlayers on open circuit voltage and carrier lifetime in thin film solar cells, *Appl. Phys. Lett.* **2016**, *108*, 113301.

(20) D. Hocine, M. Belkaïd, K. Lagha, Influence of interfacial oxide layer thickness on conversion efficiency of SnO 2 /SiO 2 /Si(N) Solar Cells, *Rev. des Energies Renouvelables* **2008**, *11*, 379.

(21) R. L. van Meirhaeghe, F. Cardon, W. P. Gomes, Effects of thin oxide layers on the characteristics of GaAs MIS solar cells, Phys. Status Solidi 1980, 59, 477.

(22) Hur, T.-B.; Hwang, Y.-H.; Kim, H.-K.; Lee, I. J. Strain Effects in ZnO Thin Films and Nanoparticles. *J. Appl. Phys.* **2006**, *99* (6), 64308.

(23) Lim, H.; Sagnes, G.; Bastide, G. A Study of the Chemical oxide/InP Interface States. *J. Appl. Phys.* **1982**, *53* (11), 7450–7453.

(24) Coutts, T. J.; Li, X.; Wanlass, M. W.; Emery, K. A.; Gessert, T. A. Hybrid Solar Cells Based on DC Magnetron Sputtered Films of n-ITO on APMOVPE Grown P-InP. 20th *IEEE Photovoltaic Specialists Conference*; IEEE, 1988; pp 660–665 vol.1.

(25) Hwang, D.-K.; Bang, K.-H.; Jeong, M.-C.; Myoung, J.-M. Effects of RF Power Variation on Properties of ZnO Thin Films and Electrical Properties of P–n Homojunction. *J. Cryst. Growth* **2003**, *254* (3), 449–455.

(26) Fan Hai-Bo, Yang Shao-Yan, Zhan Pan-Feng, Wei Hong-Yuan, Liu Xian- Lin, Jiao Chun-Mei, Zhu Qin-Sheng, C. Y.-H. W. Z.-G. Investigation of Oxygen Vacavcy and Interstitial Oxygen Defects in ZnO Films by Photoluminescence Ad X-Ray Photoelectron Spectroscopy. *Chin. Phys. Lett* **2007**, *24*, 2018.

(27) L. Tasakalakos, *Nanotechnology for Photovoltaics*, CRC Press, Taylor & Francis, **2010**, 11.

(28) Xi, L.; Cho, D. Y.; Besmehn, A.; Duchamp, M.; Grützmacher, D.; Lam, Y. M.; Kardynał, B. E. Effect of Zinc Incorporation on the Performance of Red Light Emitting InP Core Nanocrystals. *Inorg. Chem.* **2016**, *55* (17), 8381–8386.

(29) Kim, S. H.; Joo, S. Y.; Jin, H. S.; Kim, W.-B.; Park, T. J. Ultrathin ZnS and ZnO Interfacial Passivation Layers for Atomic-Layer-Deposited HfO_2 Films on InP Substrates. *ACS Appl. Mater. Interfaces* **2016**, *8* (32), 20880–20884.

(30) Elrod, U.; Lux-steiner, M. C.; Obergfell, M.; Bucher, E. Surface Chemistry of Zn3P3 Single Crystals Studied by XPS. Appl. Phys. B, **1987**, *201*, 197–201.

(31) Luber, E. J.; Mobarok, H.; Buriak, J. M. Solution-Processed Zinc Phosphide Nanocrystals for Thin Film Photovoltaic Applications. *ACS Nano* **2013**, *7* (9), 8136–8146.

(32) Crobu, M.; Rossi, A.; Mangolini, F.; Spencer, N. D. Chain-Length-Identification Strategy in Zinc Polyphosphate Glasses by Means of XPS and ToF-SIMS. *Anal. Bioanal. Chem.* **2012**, *403* (5), 1415–1432.

(33) Vasu, V.; Manivannan, P.; Subrahmanyam, A. Transport Mechanism of Spray Pyrolytic-Grown Indium Tin Oxide/indium Phosphide Junctions. *J. Appl. Phys.* **1995**, *77* (10), 5220–5224.

(34) Gouskov, L.; Luquet, H.; Gril, C.; Oemry, A.; Savelli, M. n ITO/p InP: A Photo and Electroluminescent Diode. *Rev. Phys. Appl.* **1982**, *17* (3), 125–132.

(35) Coutts, T. J.; Li, X.; Wanlass, M. W.; Emery, K. A.; Gessert, T. A. Hybrid Solar Cells Based on DC Magnetron Sputtered Films of n-ITO on APMOVPE Grown P-InP. In *Conference Record of the Twentieth IEEE Photovoltaic Specialists Conference*; IEEE, 1988; pp 660–665 vol.1.

(36) Moison, J. M.; Bensoussan, M. Electronic Properties of the InP(100) Surface. *Surf. Sci.* **1986**, *168* (1), 68–73.

(37) Schlesinger, R.; Xu, Y.; Hofmann, O. T.; Winkler, S.; Frisch, J.; Niederhausen, J.; Vollmer, A.; Blumstengel, S.; Henneberger, F.; Rinke, P.; et al. Controlling the Work Function of ZnO and the Energy-Level Alignment at the Interface to Organic Semiconductors with a Molecular Electron Acceptor. *Phys. Rev. B* **2013**, *87*.

(38) http://www.ioffe.ru/SVA/NSM/Semicond/InP/electric.html

(39) http://www.axt.com/site/index.php?q=node/36

(40) Niemegeers, A.; Burgelman, M.; Herberholz, R.; Rau, U.; Hariskos, D. Model for Electronic Transport in Cu(In,Ga)Se2 Solar Cells. *Prog. PHOTOVOLTAICS Res. Appl. Prog. Photovolt. Res. Appl. 6,* **1998**, *421* (April), 407–421.

(41) SCAPS-Materials File

(42) Zhang, P. F.; Liu, X. L.; Wei, H. Y.; Fan, H. B.; Liang, Z. M.; Jin, P.; Yang, S. Y.; Jiao, C. M.; Zhu, Q. S.; Wang, Z. G. Rapid Thermal Annealing Properties of ZnO Films Grown Using Methanol as Oxidant. *J. Phys. D. Appl. Phys.* **2007**, *40* (19), 6010–6013.

(43) Islam, M. N.; Ghosh, T. B.; Chopra, K. L.; Acharya, H. N. XPS and X-Ray Diffraction Studies of Aluminum-Doped Zinc Oxide Transparent Conducting Films. *Thin Solid Films* **1996**, *280*, 20–25.